Rapid settling of a colloidal gel

C. Derec,* D. Senis, L. Talini,† and C. Allain
Laboratoire FAST, Bâtiment 502, Campus Universitaire, 91405 Orsay Cedex, France
(Received 22 January 2003; published 23 June 2003)

We study the rapid collapse of gels formed from strongly aggregating colloidal suspensions. This gravity-driven collapse is associated with the apparition of fractures in the bulk of the gels that provide an easy route to the gel-supernatant interface for the solvent and are the cause for the strong increase of the settling velocity. We propose a model that connects the apparition of a fracture in the gel to the settling velocity of the interface. This description takes into account the microscopic structure of the gel and is consistent with the experimental results.

DOI: 10.1103/PhysRevE.67.062401 PACS number(s): 61.43.Hv

The gravity-driven collapse of gels formed from aggregating colloidal suspensions has been observed in systems in which aggregation is induced by different natures of interactions (van der Waals forces, depletion-induced attraction...) [1–5]. Despite these differences, the settling behavior of the resulting gels displays common features whose specificity has recently aroused interest. The sedimentation is characterized by the succession of three velocity regimes: after a period during which little or no settling occurs, a rapid collapse is observed that is further followed by the slow compaction of the gel. Formation of channels in the bulk of the gel as well as volcanolike structures at the gel-solvent interface has been observed in different systems during the phase of rapid collapse [1,2,5]. The origin and the mechanism of this collapse remain unclear. Although a model has recently been proposed to describe the processes involved in the sudden collapse [6], it is limited to the case of weakly aggregated suspensions in which the gel restructures under the action of thermal motion. Moreover, the link between the apparition of channels within the gel and the sudden increase in the settling velocity has not been investigated yet.

In this paper we focus on gels formed from strongly aggregating suspensions, that do not evolve under the action of thermal motion once they are formed (''permanent gels''). The particle density being large, the action of gravity can nevertheless affect the gel stability. We have shown in a previous paper [2] that the behavior of such gels depends on the particle volume fraction Φ: at small volume fractions ($\Phi < \Phi^*$), aggregates form that further settle individually, whereas at large Φ ($\Phi > \Phi^{**}$) a stable gel fills the whole cell. At intermediate values of Φ, a gel constituted by a close packing of fractal aggregates quickly forms, but it is so brittle that it further settles under the action of its own weight. The settling behavior then follows the three regimes described above. Taking into account the microscopic structure of the gel and its specific mechanical properties we have successfully modeled the first and final settling regimes in a previous work [7]. In the present work we propose a description for the settling velocity in the fast settling regime.

The colloidal particles are spherical calcium carbonate particles (radius $a = 35$ nm) that are dispersed in deionized water. A strong stirring of the suspensions during two weeks ensures that the particles are in a well-dispersed state prior to each experiment. The experimental conditions [8] are such that once in solution the particles are weakly charged, particle interactions therefore result in van der Waals attractive forces. As a consequence, the particles irreversibly aggregate as soon as the stirring of the suspension is stopped. The particle volume fraction Φ ranges from 0.4% to 0.8%, which corresponds to the intermediate range within which the formed gel settles ($\Phi^* < \Phi < \Phi^{**}$).

The settling cells are made of Plexiglas. They are of rectangular section, of useful height $H = 70$ mm and inner width $d = 12$ mm. Three cells of different lengths L have been used: a small one (inner length 30 mm), a medium one (60 mm), and a large one (120 mm). Before each experiment the cells are entirely filled with the suspension and sealed such as to eliminate the air from the sample. We thus avoid the presence of an air-suspension meniscus that could hinder the displacement of the interface. The settling of all the used suspensions (Φ ranging from 0.4% to 0.8%) has been studied in the small cell, while experiments in the medium cell were performed for $\Phi = 0.7\%$ and experiments in the large cell for $\Phi = 0.5\%$, 0.7%, and 0.8%.

The motion of the gel is recorded through a charge-coupled device (CCD) camera that takes views of the width to height plane of the cell. Space vs time diagrams are further built from the video images by placing side by side one-pixel-wide lines recorded at successive times. The line is parallel to the height of the cell and is placed at a distance $d/4$ of one side wall. The position of the interface as a function of time, $h(t)$, is extracted from the space vs time diagrams. The eruptions are located at the midwidth of the cell and can significantly deform the water-gel interface, this deformation is, however, negligible at a distance $d/4$ from the side walls, and thus does not appear on the space vs time diagrams. Side views (length to height) of the cell are also taken by another CCD camera in order to observe the apparition of eruptions at the interface.

A typical space vs time diagram is shown in Fig. 1. The position of the interface $h(t)$ is given by the frontier between the dark (supernatant) and white (gel) zones. The three successive regimes described above can be distinguished. Only

*Present address: Laboratoire PMMH, ESPCI, 10 rue Vauquelin, 75005 Paris, France.
†Corresponding author. Email address: talini@fast.u-psud.fr

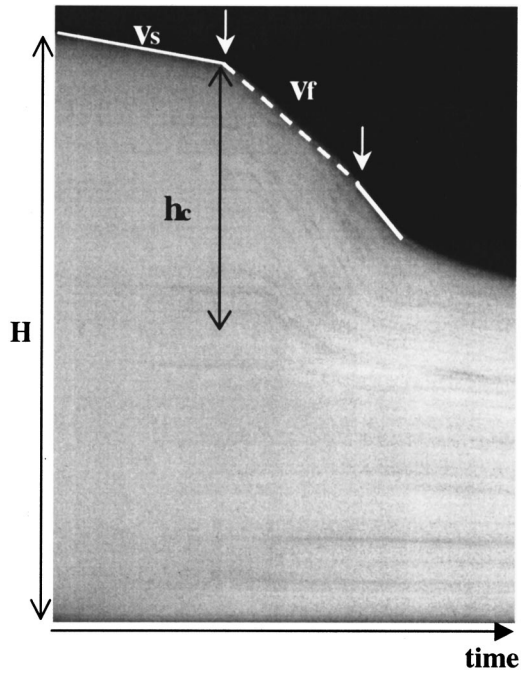

FIG. 1. Space vs time diagram of a settling gel ($\Phi = 0.5\%$). The diagram is obtained by recording a vertical single-pixel line at successive times. The dimensions of the diagram corresponds horizontally to 1770 s and vertically to 74 mm. The frontier between the dark and white zones corresponds to the water-gel interface position as a function of time. It is enhanced by a white line in the first and second settling regime. The white arrows indicate the occurrence of eruptions at the surface of the gel.

the beginning of the final regime (corresponding to the slow compaction of the gel) appears in Fig. 1. Equilibrium is reached within a time scale much larger than that of Fig. 1 (several hours). Note that owing to the fractal structure of the aggregates the final height of the sediment is large even at the moderate volume fractions we work [7]. For instance, it is of the order of half the initial suspension height for $\Phi = 0.7\%$.

Let us now focus on the first and second regimes. The gel first settles at a constant velocity v_s that depends on the volume fraction such that

$$v_s \sim \Phi^{(1-D)/(3-D)}, \tag{1}$$

where D is the fractal dimension of the aggregates [2]. Note that numerical and experimental works [9,10] have shown that D can vary with the volume fraction (although the nature of this variation is still an open matter); this variation is, however, expected to be smaller than 2% within the limited range of volume fractions we consider [9].

In the case of Fig. 1, the slow velocity is $v_s = 5.1\ \mu\mathrm{m\,s}^{-1}$. The slow settling regime is followed by the rapid collapse of the gel. The beginning of this fast regime always coincides with the apparition of a small volcanolike structure at the gel-water interface. Other eruptions can later appear, their total number depending on the cell size. Figure 1 corresponds to an experiment performed in the small cell in which two eruptions are observed as indicated (white arrows). The first one appears at the beginning of the second regime and is later followed by a second eruption. After each eruption the settling velocity is constant and is of the order of five times larger than v_s. In the case of Fig. 1, the value of the settling velocity is $v_f = 25\ \mu\mathrm{m\,s}^{-1}$ after the first eruption and $35\ \mu\mathrm{m\,s}^{-1}$ after the second one. A close side view of the interface showing the apparition of an eruption is displayed in Fig. 2. The eruptions are the signature of the opening of fractures within the gel, forming channels that provide an easy route for the upward flow of the solvent. As this flow erodes the channel, colloidal material is carried to the interface and forms the observed volcanolike structure. We have found that the number of eruptions depends on the cell geometry, whereas it remains constant when the volume fraction varies. Two eruptions are observed in the small cell. In the larger cells, the number of eruptions can slightly vary from one experiment to another: 5–7 eruptions occur in the medium cell, and 11–12 in the large cell. In all cells, the eruptions appear along a line parallel to the length of the cell and situated at a distance $d/2$ from the walls. Since it is difficult to separate the influence of the formation of the different fractures on the motion of the interface, we will herein focus on the settling velocity resulting from the apparition of a single fracture denoted as v_f.

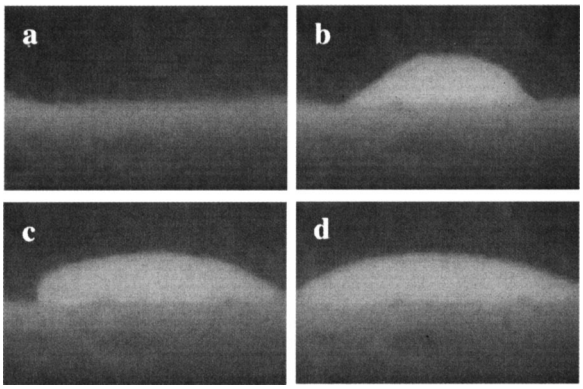

FIG. 2. Close view of an eruption at the surface of the settling gel at different successive times (a)–(d). The gel appears in gray and the supernatant in black. The width of the photographs corresponds to 7.5 mm and the time interval between two photographs is 4 s.

To model its influence on the settling kinetics, we consider a fracture as a vertical cylindrical channel of radius r_c, as schematized in Fig. 3. Similarly, to macroscopic suspensions, the settling gel can be roughly divided into two parts: a compacted sediment lying in the bottom of the cell and an upper part within which compaction is negligible. Although the particle volume fraction is larger than Φ in the bottom of the cell, it can be considered as uniform and can be taken equal to Φ in the other part. The channel of height h_c extends over the part of the gel that is not compacted at the end of the first settling regime, thus of volume fraction Φ.

Let us now describe the flow field within the gel. The solvent is assumed to freely flow upward through the fracture. As a result, in a zone centered on the fracture, the solvent is drained toward the fracture that provides an easy route to the surface. We therefore consider a zone of radius χ

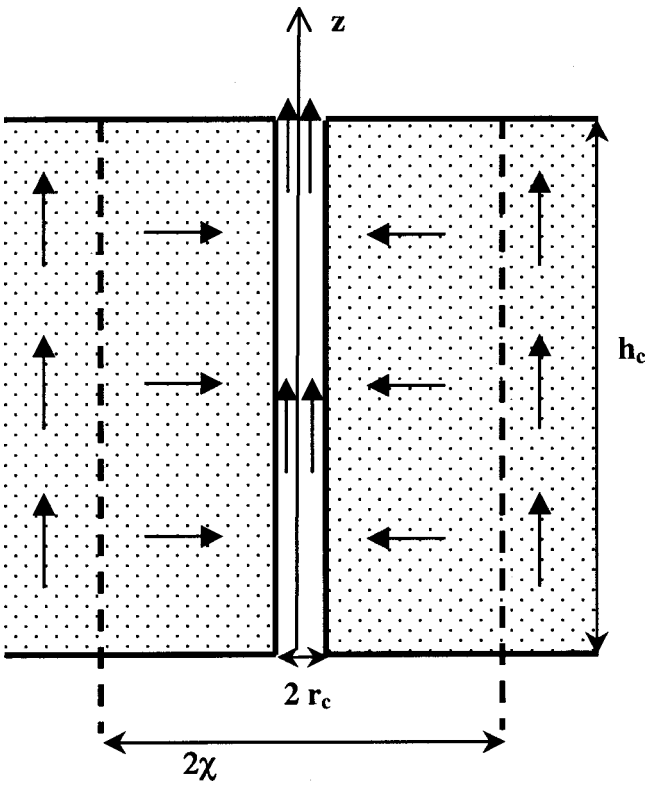

FIG. 3. Schematic representation of the fracture as considered in the proposed model. It consists of a vertical cylindrical channel of height h_c and radius r_c through which the solvent flows toward the gel-water interface. The arrows indicate the direction of the dominant flow in each region: within a cylindrical zone of radius χ centered on the fracture the flow is horizontal, whereas it remains vertical outside this zone.

such that inside this zone ($r<\chi$) the solvent flow is mainly radial. Outside this zone ($r>\chi$), the influence of the fracture is negligible and the solvent flows vertically, as it would in the absence of fractures. Let us now write the pressure gradient in the different zones.

(1) For $r>\chi$, the description is identical to that of the first settling regime that is detailed elsewhere [2,7]: considering that the close packing of fractal aggregates of size ξ that constitutes the gel is analogous to a porous medium of permeability k, the vertical component of the pressure gradient is related to velocity of the solvent in the gel frame through Darcy's law

$$\frac{dP}{dz} = -\frac{\eta}{k}(1-\Phi)(V_z + v_s), \tag{2}$$

where η is the solvent viscosity, V_z the vertical component of the solvent velocity in the laboratory frame, and v_s the absolute value of the particles velocity in the same frame. Using flow conservation, the pressure gradient can furthermore be expressed as a function of v_s only, i.e., $dP/dz = -\eta v_x/k$. Taking into account the fractal nature of the aggregates and using the relation between the permeability k and size ξ eventually yields Eq. (1), which is in good agreement with the experimental data, as shown in Fig. 4. As

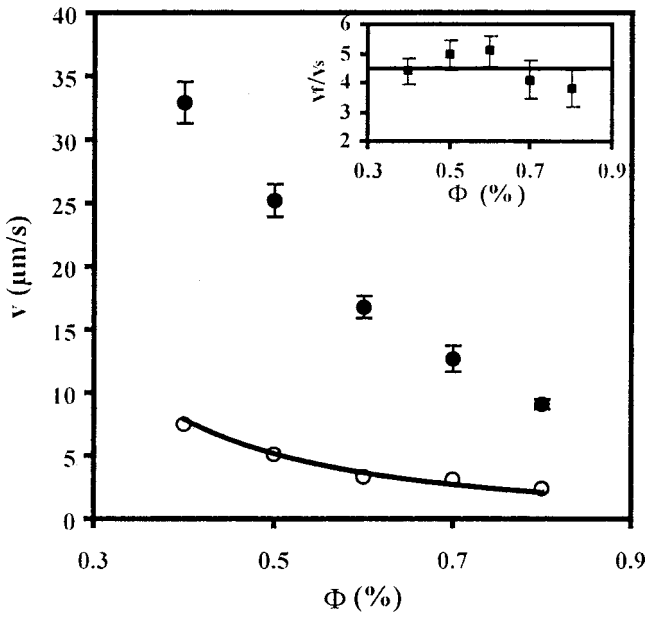

FIG. 4. Settling velocities v_s (open circles) and v_f (full circles) as a function of the particle volume fraction Φ. The experimental uncertainty upon v_s is too small to appear. The full line represents Eq. (1) with $D=2.43$. The inset shows the corresponding variations of the ratio v_f/v_s.

pointed out in what precedes, the use of a constant fractal dimension to describe the experimental data of Fig. 4 is relevant within the small range of volume fractions we are concerned with.

(2) For $r_c \leqslant r < \chi$, we assume that the radial component V_r of the solvent velocity does not depend on the height z, which corresponds to a negligible pressure loss along the fracture. The radial component of the pressure gradient follows Darcy's law such that

$$\frac{dP}{dr} = -\frac{\eta}{k}(1-\Phi)V_r(r). \tag{3}$$

Conservation of the fluid flow toward the channel yields $r_c V_r(r_c) = r V_r(r)$. Moreover, the displacement of the interface at the velocity v_f being the consequence of the flow in the channel, the flow rate in the channel is equivalent to the flow rate resulting from the settling of the zone of radius χ, i.e., $2\pi r_c h_c (1-\Phi)V_r(r_c) = -\pi\chi^2 v_f$. The radial component of the pressure gradient finally writes

$$\frac{dP}{dr} = +\frac{\eta}{k}\frac{\chi^2}{2r_c h_c}v_f. \tag{4}$$

Finally, from the definition of χ, the radial and vertical components must be equal at $r=\chi$. Using Eq. (2) and (4) we obtain a relation between the slow and fast settling velocities that writes

$$\frac{v_f}{v_s} = \frac{2h_c}{\chi}. \tag{5}$$

Let us now compare Eq. (5) to the experimental results. Figure 4 shows the variations of both settling velocities v_s and v_f as a function of Φ. The ratio v_f/v_s remains constant within the experimental uncertainty and its mean value is 4.5 for volume fractions ranging from 0.4% to 0.8%. Note that in Eq. (5), the velocity v_f represents the interface velocity in the vicinity of the fracture, whereas experimentally we measure a mean velocity of the interface in the whole cell. However, since the velocity v_f is much larger than v_s and the experiments of Fig. 4 have been performed in the smaller cell, the values of the mean and local velocities are very close.

In order to check the validity of Eq. (5), we have estimated the distance χ and height h_c. An evaluation of χ is provided by the observation of the spatial location of the eruptions in the different cells. Since χ represents the radius of the zone of influence of a fracture, two eruptions are expected to be separated by a distance larger than χ. We have found in all cells that the distance separating active eruptions is 12 ± 2 mm. This value being consistent with the fact that only one eruption occurs along the width $d=12$ mm of the cells, we thus estimate that $\chi=12\pm2$ mm. The height h_c can be deduced from the space vs time diagrams, as shown in Fig. 1, small cracks indicated by darker lines appear at the cell wall. These cracks slowly evolve with time at the bottom of the cell, whereas they reproduce the fast interface motion in the upper part of the gel. We identify h_c with the height of the gel that follows this fast motion and we have systematically measured it from the space vs time diagrams. We have thus found that $h_c=30\pm3$ mm, which gives $2h_c/\chi=5\pm1$. This value is in good agreement with that found for the ratio v_f/v_s, which shows the relevancy of the model we propose. Note that the channel radius r_c can moreover be estimated from the gel properties. It is found to be of the order of a few hundreds of micrometers, which is consistent with the experimental observations and further validates the model.

Using a simple hydrodynamical model allowed us to describe the increase in the settling velocity of a colloidal gel caused by the apparition of fractures within the gel. The description we propose could be compared to experimental results obtained with other colloidal systems that exhibit similar settling behavior.

''Laboratoire Fluides, Automatique et Systèmes Thermiques'' is a laboratory of Universities Paris VI and Paris XI and of CNRS (UMR 7608).

[1] G. G. Glasrud, R. C. Navarrete, L. E. Scriven, and C. W. Macosko, AIChE J. **39**, 560 (1993).
[2] C. Allain, M. Cloître, and M. Wafra, Phys. Rev. Lett. **74**, 1478 (1995).
[3] A. Parker, A. P. Gunning, Ng Kim, and M. M. Robins, Food Hydrocolloids **9**, 333 (1995).
[4] N. A. M. Verhaeg, D. Asnaghi, and H. N. W. Lekkerkerker, Physica A **264**, 64 (1999).
[5] L. Starrs, W. C. K. Poon, D. J. Hibberd, and M. M. Robbins, J. Phys.: Condens. Matter **14**, 2485 (2002).
[6] R. M. L. Evans and L. Starrs, J. Phys.: Condens. Matter **14**, 2507 (2002).
[7] D. Senis, L. Gorre-Talini, and C. Allain, Eur. Phys. J. E **4**, 59 (2001).
[8] D. Senis, Ph.D. thesis, University Paris VI, 1998.
[9] M. Lach-hab, A. E. Gonzalez, and E. Blaisten-Barojas, Phys. Rev. E **54**, 5456 (1996); **57**, 4520 (1998).
[10] M. Lattuada, H. Wu, and M. Morbidelli, Phys. Rev. E **64**, 061404 (2001).